

Supporting Information

Indications for a universal hydrogen catalysis mechanism in [FeFe]-hydrogenases of different phylogenetic groups

Moritz Senger^{1,2}*, Conrad Schumann¹, Princess R. Cabotaje¹, Afridi Zamader^{1, †}, Ping Huang¹, Henrik Land¹ and Gustav Berggren^{1, *}

1) Department of Chemistry – Ångström Laboratory, Molecular Biomimetics, Uppsala University, 75120 Uppsala, Sweden

2) Department of Chemistry – Bio Medical Centre, Biochemistry, Uppsala University, 75120 Uppsala, Sweden

[†]) Current address: Laboratoire d'Electrochimie Moléculaire (LEM), Université Paris Cité, CNRS, F-75006, Paris, France.

*To whom correspondence should be addressed

moritz.senger@kemi.uu.se and gustav.berggren@kemi.uu.se

Contents

Materials and Methods	2
Transmission-FTIR Spectroscopy	2
ATR-FTIR spectroscopy	2
EPR spectroscopy	2
Enzyme purification	2
Synthesis of diiron site mimics	3
<i>TamHydS</i> protein structure determination	4
Figure S1: Catalytic cycle models including H_{red}^* and H_{sred}^*	5
Figure S2: Absolute spectra of the H_{ox} to H_{red}' transition and H_{ox} to H_{red}' transition kinetics in <i>TamHydS</i> ^{PDT}	6
Figure S3: Comparison of the H_{ox} to H_{red}' transition in <i>TamHydS</i> ^{PDT} samples in the presence and absence of sodium dithionite (NaDT) reveals no influence of NaDT on the transition.	7
Figure S4: Zoom in on the H_{ox} to H_{red}' transition kinetics in <i>TamHydS</i> ^{PDT}	8
Figure S5: Unscaled kinetics of the H_{ox} to H_{red}' transition in <i>TamHydS</i> ^{PDT}	9
Figure S6: Absolute spectra at 0 seconds, 44 seconds and 220 seconds of illumination (top), and the full series of difference spectra (bottom) for the photoreduction of <i>TamHydS</i>	10
Figure S7: Absolute infrared spectra of di-iron site mimics featuring different combinations of carbonyl, phosphine and cyanide ligands.	11
Figure S8: The effect of photoreduction on the accessory [4Fe4S] clusters of <i>TamHydS</i> monitored by EPR spectroscopy.	12
Figure S9: Overview of the infrared bands of <i>TamHydS</i> ^{ADT} and <i>TamHydS</i> ^{PDT} [FeFe]-hydrogenase observed in various redox states.	13
Fit parameters	14
Supporting References	16

Materials and Methods

Transmission-FTIR Spectroscopy

The characterization of diiron cofactors was recorded using infrared spectroscopy via transmission mode in a Bruker Vertex V70v spectrometer. 4-6 mg of each sample was dissolved in 100 μL of degassed CH_3CN and injected inside a transmission cell made of CaF_2 with a spacer of 0.05 mm thickness for the spectroscopic analysis. The sample preparation was conducted inside glovebox to avoid any oxygenic degradation.

ATR-FTIR spectroscopy

Attenuated Total Reflectance Fourier-Transform Infrared (ATR-FTIR) spectroscopy. A solution of 4 μL enzyme (0.2–1 mM *TamHydS*) in 10 mM Tris buffer (pH 8.0), 1 μL Eosin Y (6mM) and 1 μL 100 mM Triethanolamine (TEOA) was deposited on the ATR crystal in the anaerobic atmosphere of a MBraun Glove box. In the case of *TamHydS*^{PDT} 1 μL of 241 μM *TamHydS*^{PDT} in 10 mM Tris buffer (pH 8.0), 1 μL 1mM Eosin Y and+1 μL 100mM TEOA was used. The ATR unit (BioRadII from Harrick) was sealed with a custom build PEEK cell that allowed for gas exchange and illumination (similar to Stripp 2021¹ and Senger et al., 2016²) mounted in a FTIR spectrometer (Vertex V70v, Bruker). Illumination for photo-reduction experiments was facilitated via a Schott KL2500 lamp optically coupled to the ATR crystal surface with fiber optics. The sample was dried under 100% nitrogen gas and rehydrated with a humidified aerosol (100 mM Tris-HCl, pH 8) as described before.³

For H_2 exposure experiments a mixed buffer (pH 8, 50mM TRIS-HCL, 50 mM Citric acid) was used. Spectra were recorded with 2 cm^{-1} resolution, a scanner velocity of 80 Hz and averaged of varying number of scans (mostly 1000 scans). All measurements were performed at ambient conditions (room temperature and pressure, hydrated enzyme films). Gases (N_2 , H_2) were applied at a flow rate of 0.5-1.5 L/min. The data was analysed and plotted to our protocols described previously.^{4,5}

All identified peaks have a minimal signal to noise ratio of >4.

EPR spectroscopy

X-band EPR measurements were performed on a Bruker ELEXYS E500 spectrometer equipped with a SuperX EPR049 microwave bridge and a cylindrical TE_{011} ER 4122SHQE cavity in connection with an Oxford Instruments continuous flow cryostat. Measuring temperatures were achieved using liquid helium flow through an ITC 503 temperature controller (Oxford Instruments). The Xepr software package (Bruker) was used for data acquisition and processing. EasySpin software version easyspin-6.0.0-dev.51 was used for spectral simulation and fitting.^{6,7} All spectra were recorded at the following settings: modulation frequency 100 kHz, amplitude 10 G; microwave frequency 9.4 GHz, power 80 μW and $T=10$ K. EPR Samples containing 50 μM *TamHydS*, 150 μM Eosin Y and 1 mM TEOA were prepared in 100 mM Tris-HCl, pH 8.0 under dim white light in a neat argon atmosphere. The samples were subsequently either wrapped in Al-foil to minimize light exposure (“dark samples”) or irradiated inside the EPR tube for an hour using a Schott KL2500, prior to freezing.

Enzyme purification

Preparation of *TamHydS*^{ADT}

The preparation of *TamHydS*^{ADT} was performed as previously reported with minor changes to the procedure.⁸ For the expression of the apo-form, sequence-confirmed plasmids were transformed in chemically competent *E. coli* BL21(DE3) cells. The protein expression was induced at $\text{O.D.}_{600} \approx 0.5$ with 1 mM IPTG with concomitant supplementation of the culture with 100 μM FeSO_4 in 1% HCl solution. The harvested cell pellets were lysed by 3 cycles of freezing/thawing in liquid N_2 in 100 mM Tris-HCl,

150 mM NaCl pH 8.0 supplemented with 1 g/L lysozyme, 0.05 g/L DNase, 0.05 g/L RNase, 2 g/L MgCl₂ * 6 H₂O and cComplete™ Protease Inhibitor Cocktail (Roche). The cell lysis, protein purification, the reconstitution of the [4Fe-4S] clusters, as well as the activation of the enzyme were carried out in an MBraun glovebox under argon atmosphere (app. 1 ppm O₂). The protein was purified using StrepTrap affinity chromatography (StrepTrap HP (GE Healthcare)) following the manufacturer's instructions and applying an additional washing step with 1 M urea in 100 mM Tris-HCl, 150 mM NaCl pH 8.0. After purification, the protein yield was 2.8 mg L⁻¹ of cell culture with an iron/protein content of 11.8 Fe/protein. By incubating the enzyme (50 μM) in a reaction with 500 μM dithiothreitol, 500 nM cysteine desulfurase (E. coli IscS), 525 μM L-cysteine and 525 μM (NH₄)₂Fe(SO₄)₂(H₂O)₆ in 100 mM Tris-HCl, 150 mM NaCl pH 8.0 all [4Fe-4S] clusters were fully reconstituted (17.0 ± 1.4 Fe/protein). Subsequently, the yielded apo-form of *TamHydS* (200 μM) was semi-artificially activated by incubating it for 30 min with 4 mM sodium dithionite and 2.4 mM of [2Fe]^{ADT} in 100 mM Tris-HCl, 150 mM NaCl pH 8.0. Eventually the activation reaction was desalted using 10 mM Tris-HCl pH 8.0 containing 5 mM NaDT. The generated holo-form of [2Fe]^{ADT}-activated *TamHydS* aliquots were concentrated to 2.0 mM. Aliquots were prepared in air-tight vials and flash frozen in liquid N₂ and stored at -80 °C. The successful activation and the correct cofactor integration were verified by ATR-FTIR analyses.

Preparation of *TamHydS*^{PDT}

The preparation of *TamHydS*^{PDT} was performed as previously reported with minor changes to the procedure.⁸ For the expression of the apo-form, sequence-confirmed plasmids were transformed in chemically competent *E. coli* BL21(DE3) cells. The protein expression was induced at O.D.₆₀₀ ≈ 0.5 with 1 mM IPTG with concomitant supplementation of the culture with 100 μM FeSO₄ in 1% HCl solution. The harvested cell pellets were lysed by sonication in 100 mM Tris-HCl, 150 mM NaCl pH 8.0 supplemented with 1 g/L lysozyme, 0.05 g/L DNase, 0.05 g/L RNase, 2 g/L MgCl₂ * 6 H₂O, cComplete™ Protease Inhibitor Cocktail (Roche), 5 g/L sodium deoxycholate and 50 g/L Succrose. The cell lysis, protein purification, the reconstitution of the [4Fe-4S] clusters, as well as the activation of the enzyme were carried out in an MBraun glovebox under argon atmosphere (app. 1 ppm O₂). The protein was purified using StrepTrap affinity chromatography (StrepTrap HP (GE Healthcare)) following the manufacturer's instructions and applying an additional washing step with 5 mM ATP and 10 mM MgCl₂ in 100 mM Tris-HCl, 150 mM NaCl pH 8.0 for the removal of contaminant Hsp70 molecular chaperones.^{9,10} After elution and concentration of the enzyme a second purification step was required due to small molecular weight impurities. Therefore, a size-exclusion chromatography (Superdex 200 HP (GE Healthcare)) was carried out for the removal of the impurities. After the two purification steps, the protein yield was 0.47 mg L⁻¹ of cell culture with an iron/protein content of 8 Fe/protein. By incubating the enzyme (50 μM) in a reaction with 500 μM dithiothreitol, 500 nM cysteine desulfurase (E. coli IscS), 700 μM L-cysteine and 700 μM (NH₄)₂Fe(SO₄)₂(H₂O)₆ in 100 mM Tris-HCl, 150 mM NaCl pH 8.0 all [4Fe-4S] clusters were fully reconstituted (16.5 ± 0.4 Fe/protein). Subsequently, the yielded apo-form of *TamHydS* (50 μM) was semi-artificially activated by incubating it for 2 h with 1mM sodium dithionite and 600 μM of [2Fe]^{PDT} in 100 mM phosphate buffer pH 6.8. Eventually the activation reaction was desalted using 10 mM Tris-HCl pH 8.0 without additional NaDT. The generated holo-form of [2Fe]^{PDT}-activated *TamHydS* aliquots were concentrated to 241 μM. Aliquots were prepared in air-tight vials and flash frozen in liquid N₂ and stored at -80 °C. The successful activation and the correct cofactor integration were verified by ATR-FTIR analyses.

Synthesis of diiron site mimics

The synthesis of (Et₄N)[Fe₂(μ-PDT)(CO)₅(CN)], (Et₄N)₂[Fe₂(μ-PDT)(CO)₄(CN)₂] and (Et₄N)[Fe₂(μ-PDT)(CO)₄(CN)(P(CH₃)₃)],¹¹ (Et₄N)[Fe₂(μ-ADT)(CO)₅(CN)]¹² and (Et₄N)₂[Fe₂(μ-ADT)(CO)₄(CN)₂]¹³ were

performed using previously reported protocols, and purity verified using a combination of FTIR, NMR and UV/Vis spectroscopy.

Synthesis of $(Et_4N)[Fe_2(\mu-ADT)(CO)_4(CN)(P(CH_3)_3)]$

150 mg (0.37 mM) of $Fe_2(\mu-ADT)(CO)_6$ and 42 mg (0.56 mM) of $(CH_3)_3NO$ were added to a 100 mL of dried and deaerated Schlenk flask, following the additions the atmosphere was further deaerated with three consecutive vacuum-argon cycles. Subsequently, 24 mL of anhydrous and deaerated CH_3CN was added to the mixture to form a blood red coloured homogenous solution. Then a solution containing 58 μ L of $P(CH_3)_3$ dissolved in 8 mL of CH_3CN under argon was prepared and transferred to the former Schlenk flask dropwise over a course of 5 min and stirred the resulting mixture for one hour at room temperature (293-298 K) under argon. The complete consumption of $Fe_2(\mu-ADT)(CO)_6$ and resulting formation was $Fe_2(\mu-ADT)(CO)_5(PMe_3)$ was validated by infrared spectroscopy of the resulting mixture showing loss of peaks at 2073, 2034, 1994 cm^{-1} and parallel appearance of new peaks 2037, 1979, 1961, 1920 cm^{-1} . After one hour, the mixture was cooled to $-40^\circ C$ and treated with 58 mg (0.37 mM) of $(C_2H_5)_4NCN$ dissolved in 8 mL of CH_3CN under argon. The resulting mixture was allowed to warm back to room temperature and stirred for 30 minutes to form a dark red /brown mixture. After 30 min stirring, the reaction was terminated and solvent was evaporated under reduced pressure to yield a red coloured residue. Then the produced residue was re-dissolved in 10 mL of deaerated THF and filtered via cannula. The resulting filtrate was concentrated to less than 1 mL volume. Then, 3 mL of dry and deaerated diethyl ether was added very gently to the solution to crash out the product upon standing at $-20^\circ C$ overnight. The ether-THF mixture was subsequently removed gently and the solid crude product was washed with dry and degassed diethyl ether (10 mL \times 5). After drying under reduced pressure a dark red/brown coloured solid product was obtained. Yield: 111 mg (52%). 1H NMR (500 MHz, CD_3CN): δ 3.16 (m, 12H; 8H from $N^+CH_2CH_3$ from counter cation and 4H from NHC_2H_4 bridge), 1.44-1.37 (m, 9H, $-P(CH_3)_3$), 1.23 (m, 12H, $N^+CH_2CH_3$). ^{31}P NMR (500 MHz, d_6 -DMSO): δ 32.59. FTIR (CH_3CN): ν_{CN}) 2082 ; ν_{CO}) 1973, 1933, 1897, 1881 cm^{-1} . UV-Vis (CH_3CN): 217 nm (π - π^* , sharp), 349 nm (MLCT, sharp).

***TamHydS* protein structure determination**

The homology model of the truncated *TamHydS* was performed using YASARA Structure version 18.3.23 as previously described.^{8, 14} The homology model did not yield a structure for the C-terminal domain due to the lack of a crystal structure for reference. Conversely, AlphaFold2 predicted the C-terminal domain with the fourth [4Fe-4S] cluster visualized by extracting a [4Fe-4S] cluster with cysteine ligands from the Cpl structure (PDB ID 4XDC¹⁵) and manually integrating it into the AlphaFold2 model of *TamHydS*, binding to cysteines C379, C382, C387, and C404 via PyMOL version 2.5.4. The YASARA and AlphaFold models have an RMSD alignment = 3 Å, suggesting similar overall structure, but with variations in atomic placements and rotamers of amino acid side chains. RMSD values also indicate closer alignment of the homology model (1.541 Å) than the AlphaFold model (3.692 Å) with Cpl.

We have previously presented the mainly very high model confidence figure for the AlphaFold2 model of *TamHydS* in the SI Figure S2C of our prior study.¹⁶ Alignment of the AlphaFold2 model with the homology model resulted in an RMSD = 3 Å, indicative of an overall similar structure but with variations in atomic placements and rotamers of amino acid side chains. Compared with the crystal structure of Cpl (PDB ID 4XDC¹⁵), the RMSD values were found to be 3.692 Å and 1.541 Å for the AlphaFold2 and the homology models, respectively.

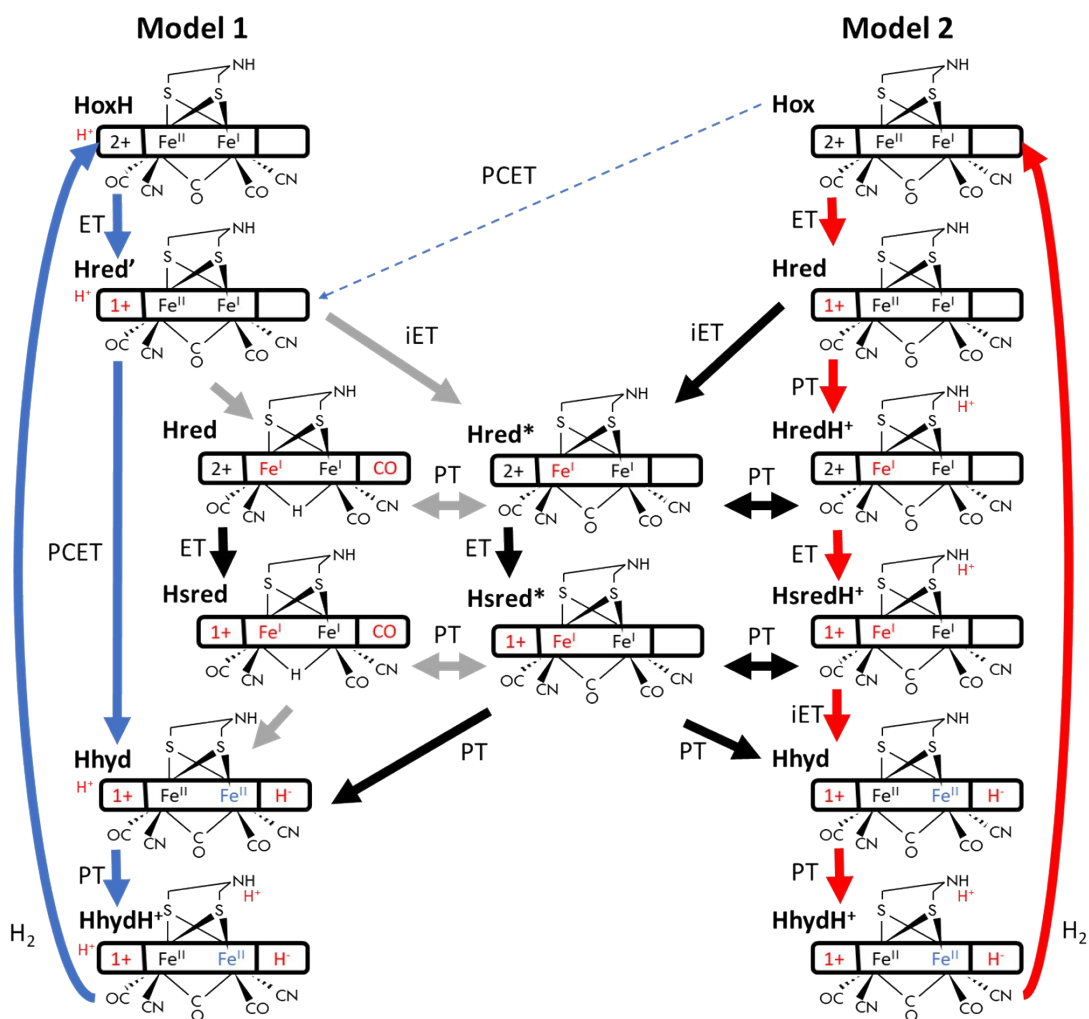
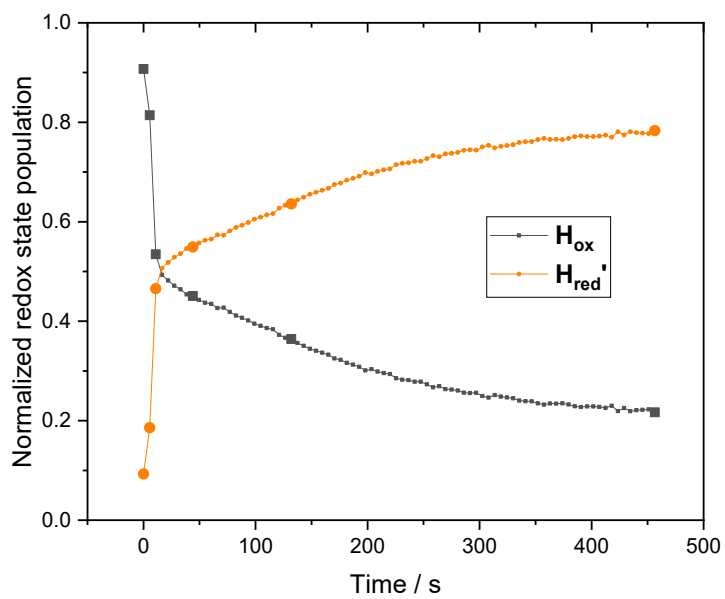
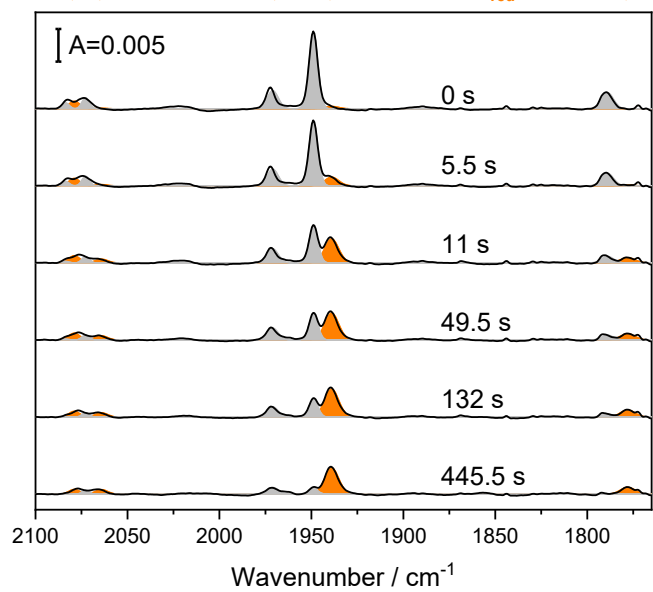


Figure S1: Catalytic cycle models including H_{red}^* and H_{sred}^* . The proposed structures for H_{red}^* and H_{sred}^* are shown in the middle. Model 1 blue arrows, Model 2 red arrows, grey arrows indicate ligand rotation. The CO ligand occupying the apical vacancy and bound protons are indicated in red. Electron transfer (ET), internal electron transfer (iET), proton transfer (PT) and proton coupled electron transfer (PCET) steps are indicated at the arrows. Red letters indicate the site of reduction, blue letters the site of oxidation relative to the oxidized state (H_{ox}).

2084	2073	1971	1949	H_{ox} 1789
2079	2064	1969	1939	H_{red}' 1778



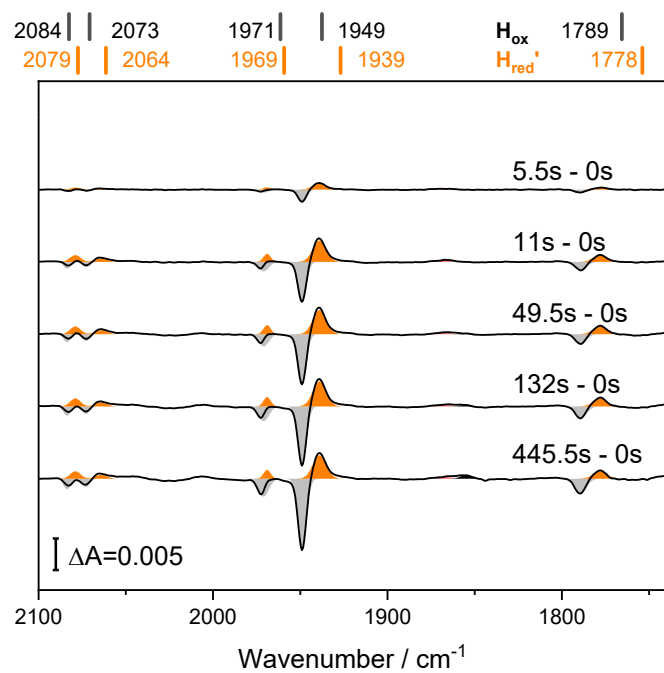


Figure S2: Absolute spectra of the H_{ox} to H_{red}' transition, H_{ox} to H_{red}' transition kinetics and difference spectra of this transition in $TamHydS^{PDT}$. The absolute spectra (top) show a nearly complete transition from H_{ox} into H_{red}' . Bold dots in the kinetics (middle) indicate the spectra displayed in Fig.S2A. The bottom graph displays the difference spectra computed of the absolute spectra in the top graph of Fig.S2.

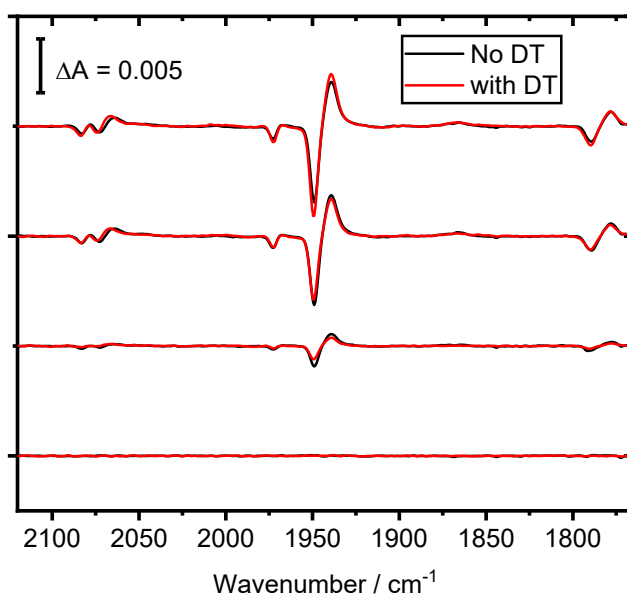
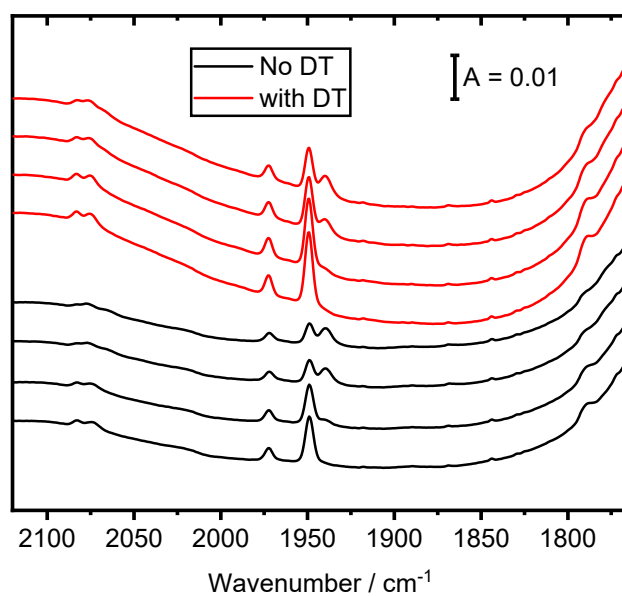


Figure S3: Comparison of the H_{ox} to H_{red}' transition in $TamHydS^{PDT}$ samples in the presence and absence of sodium dithionite (NaDT) reveals no influence of NaDT on the transition. (top) The first four absolute spectra of the cofactor region during illumination for samples with NaDT (in red) and without NaDT (in black). (bottom) The resulting difference spectra for the same transition show nearly identical behaviour.

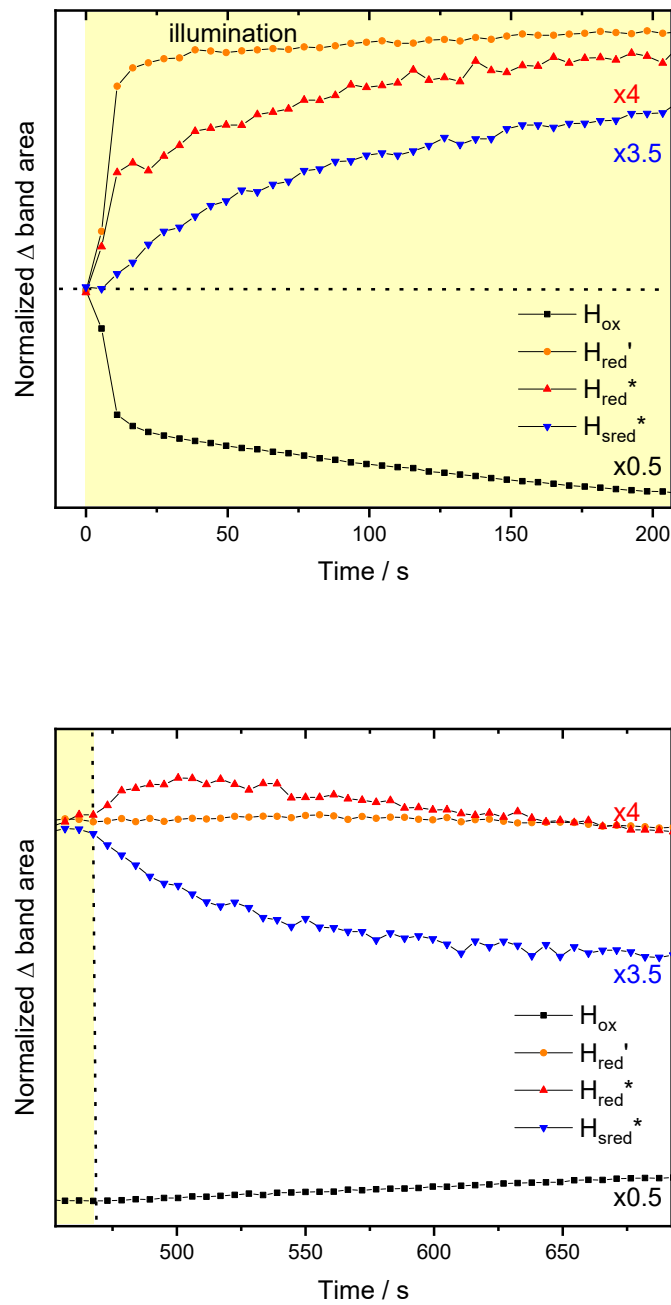


Figure S4: Zoom in on the H_{ox} to H_{red}' transition kinetics in $TamHydS^{PDT}$. (top) Upon illumination the oxidized state depopulates in favor of the reduced state H_{red}' within the first 10-15 seconds. On the same timescale half of H_{red}^* gets populated. H_{sred}^* populates on a longer timescale and after an 5-10 second lag phase. (bottom) Directly after illumination H_{sred}^* depopulates and a transient population of H_{red}^* is observed. H_{red}' and H_{red}^* then convert back into H_{ox} on a longer timescale. Note that the populations are normalized (compare Fig.S4).

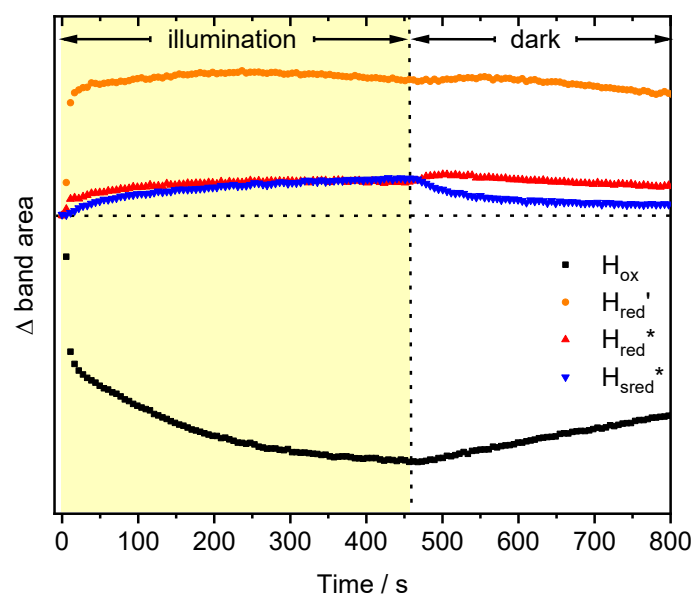
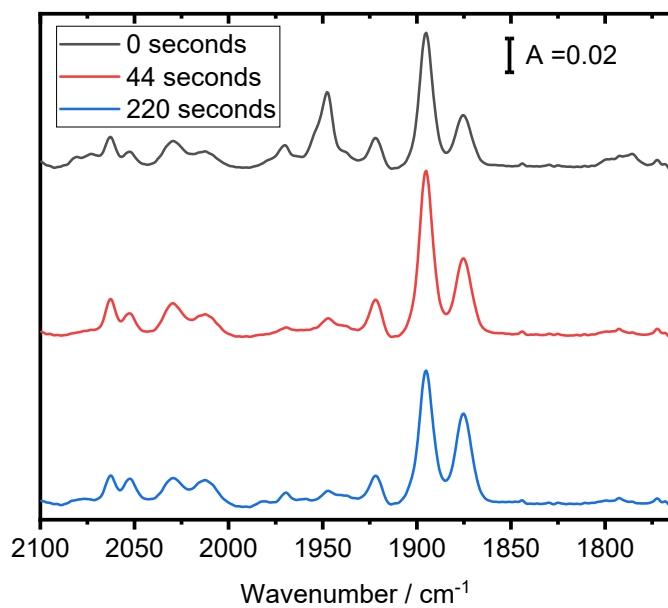
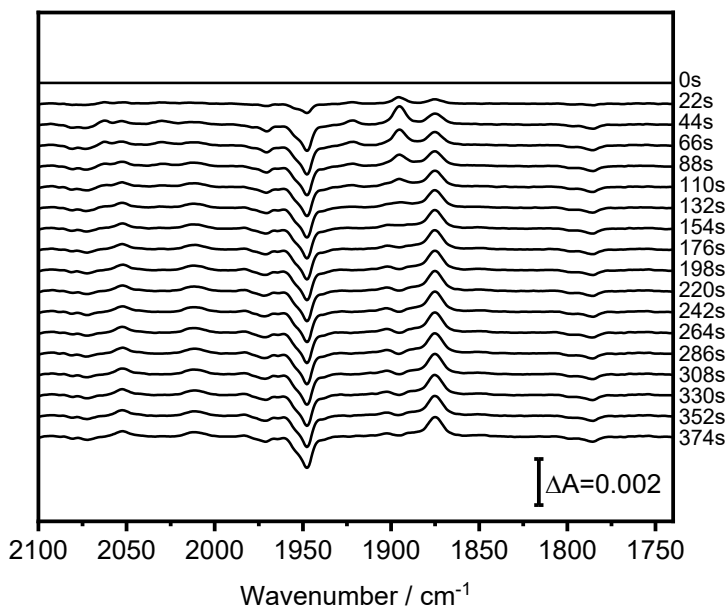


Figure S5: Unscaled kinetics of the H_{ox} to H_{red}' transition in $TamHydSPDT$. As indicative from the difference spectra in Fig.2 of the main script the unscaled kinetic further highlight that H_{red}^* and H_{sred}^* are minor species in the H_{ox} to H_{red}' transition.

A



B



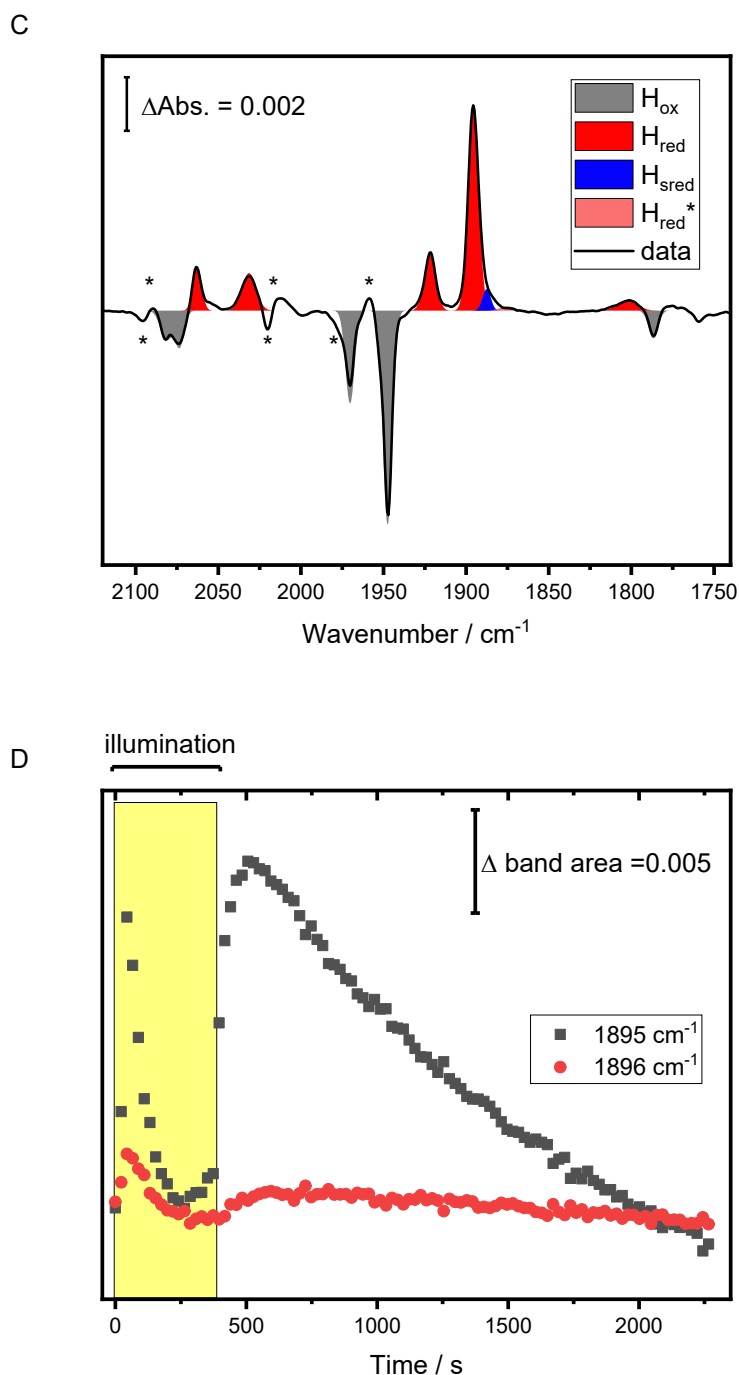


Figure S6: Absolute spectra at 0 seconds, 44 seconds and 220 seconds of illumination (A), and the full series of difference spectra (B) for the photoreduction of *TamHydS*. The difference spectra at 44 seconds and 220 seconds are shown in Fig.3 of the main text alongside with the difference of these two spectra. (C) Difference spectrum of photoreduction at lower pH than 8. Sample composed of 2 μ l *TamHydS* in 10mM Tris pH 8, 1 μ l Eosin Y in 10mM Tris pH 8 and 4 μ l TEOA in 100mM BisTris pH 6.0. Albeit not determined in the experiment, this mixed sample should result in a pH lower than 8. Under photoreduction conditions we observe mainly H_{red} formation with a minor species of H_{sred} being formed. Lower pH seems to suppress the formation of H_{red}^*/H_{sred}^* as expected. The * symbol in the graph indicates traces of air induced species $H_{air-ox}/H_{air-red}$ as described in Land et al.⁸ (D) Band area changes obtained when fitting H_{red} during and after the photo-reduction experiment with two peaks

at 1895 and 1896 cm^{-1} simultaneously. We observe the peak at 1895 cm^{-1} (black dots) as the dominant species while the signal for the 1896 cm^{-1} peak (red dots) is minor. Since the kinetics are similar to each other it is tempting to assign the band area of the 1896 cm^{-1} peak to be originating from the flanks of the major peak at 1895 cm^{-1} . If the band intensity observed at 1896 cm^{-1} would be attributed to a H_{red} species with oxidised F-clusters we would expect inverted kinetics. e.g. H_{red} reduced F-clusters get populated = H_{red} oxidised F-clusters get de-populated.

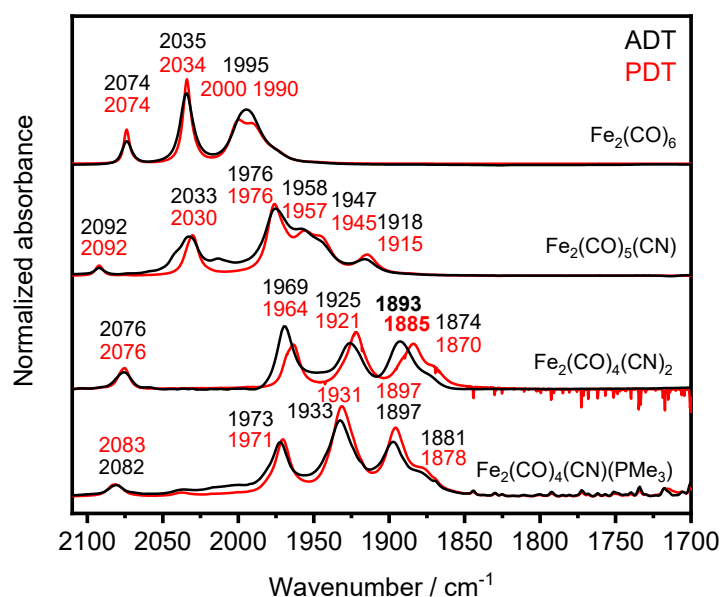
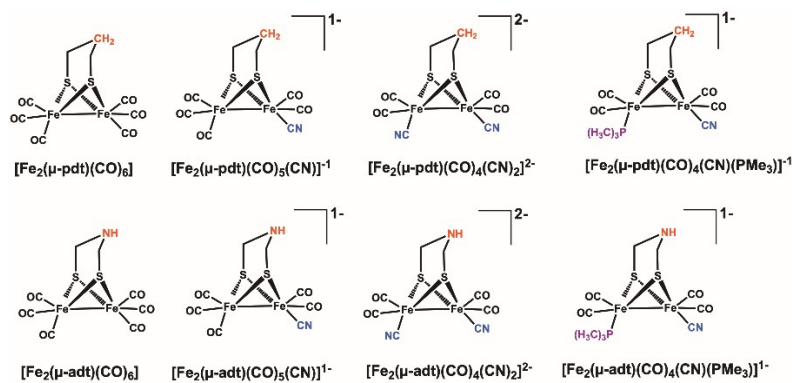


Figure S7: Absolute infrared spectra of di-iron site mimics featuring different combinations of carbonyl, phosphine and cyanide ligands.

(top) Structures of the diiron site mimics investigated. (bottom) The spectra of ADT (black) and PDT (red) versions of di-iron site mimics are plotted on top of each other. Most band positions are nearly identical for $\text{Fe}_2(\text{CO})_6$, $\text{Fe}_2(\text{CO})_5(\text{CN})$, and $\text{Fe}_2(\text{CO})_4(\text{CN})(\text{PMe}_3)$ when comparing between ADT and PDT. The dicyanide mimic $\text{Fe}_2(\text{CO})_4(\text{CN})_2$ show larger shifts between ADT and PDT version. In particular the main low wavenumber band is shifted by 8 cm^{-1} to lower wavenumbers in the PDT version (bold peak labels). This is reminiscent of the shifts observed for H_{red}^* and H_{sred}^* in *TamHydS* in either the ADT or PDT version as well as the respective shifted signatures observed in Group C [FeFe]-hydrogenase (*TmHydS*) by Chongdar et al.¹⁷

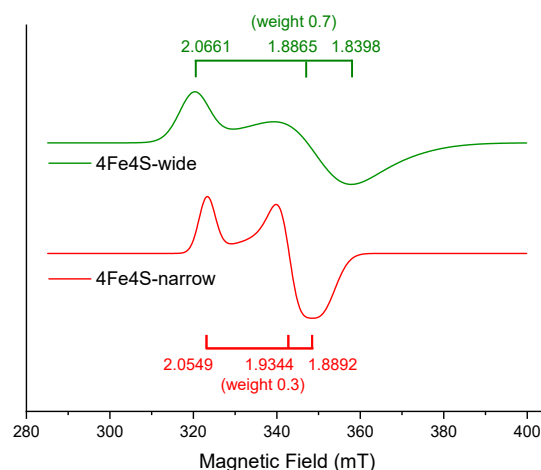
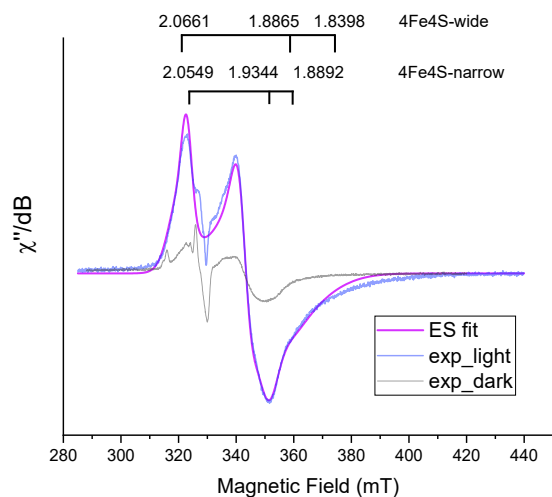


Figure S8: The effect of photoreduction on the accessory [4Fe4S] clusters of *TamHydS* monitored by EPR spectroscopy.

(Top): X-band EPR spectra collected of *TamHydS* after 5 min of photoreduction (blue spectrum) or incubation in darkness (grey spectrum), a spectral simulation of the photo-reduced sample consisting of two rhombic components is shown as an overlay (purple spectrum). For photoreduction 50 μM of holo-*TamHydS* activated with $[2\text{Fe}]^{\text{ADT}}$ was prepared with 150 μM Eosin Y, 1 mM TEOA in 100 mM Tris-HCl, pH 8.0 and either illuminated or dark-incubated. EPR settings: T 10 K; Modulation frequency 100 kHz, amplitude 10 G; Microwave frequency 9.4 GHz, power 80 μW . G-values of two rhombic signals based on simulated spectrum given above as $g_{1,2,3}$ for two 4Fe4S clusters, one narrow and one wide. **(Bottom):** Individual spectral components of the simulated spectrum shown in the Top panel. Photoreduction yields a spectrum dominated by two broad rhombic EPR signals, with g-values in good agreement with $[4\text{Fe-4S}]^+$ species. The narrow [4Fe-4S] cluster signal with $g_{1,2,3} = 2.055; 1.934$ and 1.889 (red spectrum, weight 0.3 of total signal) is highly similar to the species also observed after H_2 or dithionite treatment.⁸ The wide 4Fe4S cluster signal with $g_{1,2,3} = 2.066; 1.8865$ and 1.840 is the main component (green spectrum, weight 0.7 of total signal) and has not been observed in holo-*TamHydS* before. This shows that photoreduction yields a form of the enzyme with distinct differences in [4Fe4S] redox state populations relative to either dithionite or H_2 treatment.

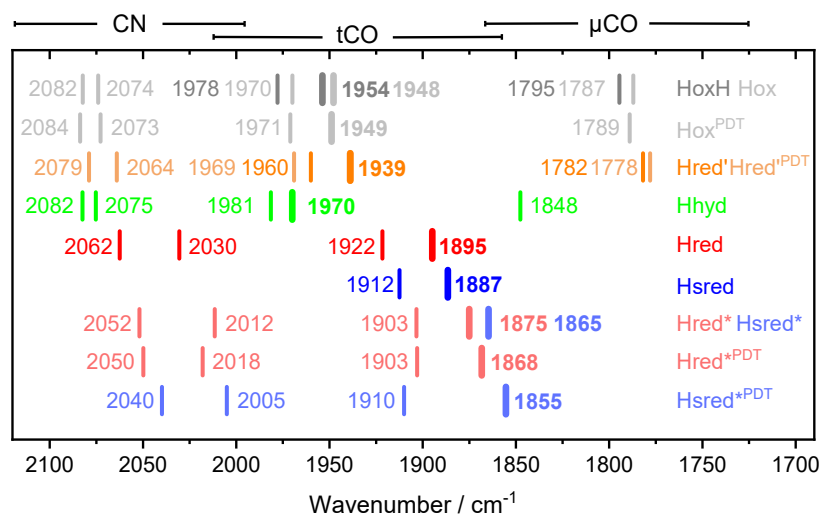


Figure S9: Overview of the infrared bands of *TamHydS*^{ADT} and *TamHydS*^{PDT} [FeFe]-hydrogenase observed in various redox states. Bold lines indicate the most intense band (most likely mainly the distal terminal CO band). For diiron site reduced states no μ CO or tCO band originating from a former μ CO ligand is detected via the photoreduction protocol.

Fit parameters

Fit parameters used to analyze and plot the data as described before.^{4, 5} In short band position and band width (Full Width Half Max (FWHM)) for each redox state are fitted to sets of spectra. In some cases, the relative amplitudes of the peaks related to one redox state are derived from the fit.

TamHydS^{PDT} Figure 2, Fig.S2

Band position	FWHM	Redox state
2083.72026	4.68229	Hox
2072.75368	4.72335	Hox
1971	7.08175	Hox
1948.87743	5.7979	Hox
1788.99337	7.69159	Hox
2064.0718	7.84682	Hred'
1969	4.83311	Hred'
1938.95605	9.04327	Hred'
1778.02679	9.36101	Hred'
2078.93592	7	Hred'
1868.3124	10	Hred*
2017.97895	7.71929	Hred*
1903	10	Hred*
2049.84462	7	Hred*
1910	10	Hsred*
1855.41198	10	Hsred*
2005.06089	10.02528	Hsred*
2039.85415	7	Hsred*

TamHydS^{ADT} Figure 3

Band position	FWHM	Redox state	Relative amplitude
1894.87489	7.29618	Hred	1
1921.60701	7.45506	Hred	0.19668
2030.49723	13.54969	Hred	0.16634
2062.46178	6.99923	Hred	0.17797
1875.04364	10.40557	Hred*	1
1903.33027	7.89636	Hred*	0.1925
2011.52926	12.20063	Hred*	0.24061
2051.92402	8.88997	Hred*	0.28125
1953.79304	8	HoxH	1
1977.85492	8	HoxH	0.28212
1794.52636	7.5	HoxH	0.2224
1787.03555	7.5	Hox	0.18394
1947.83847	6.52573	Hox	1
1969.86901	9	Hox	0.36447
2074.05355	8.77257	Hox	0.18372
2082.33957	7.50004	Hox	0.13168
2082.48876	7.5	Hhyd	-2.44937E-4
1981.4	7.5	Hhyd	-3.26908E-4
1847.66722	8	Hhyd	-1.6351E-4
1969.94397	6	Hhyd	-4.96367E-4
2075.2775	7.5	Hhyd	-1.97168E-4
1959.49346	7.5	unassigned	
1938.82419	8	Hred'	1
1781.86063	7.85505	Hred'	0.28
1960	6.67269	Hred'	0.22
1886.50156	6.86615	Hsred	1
1912.42289	5.05039	Hsred	0.24008
1864.71635	8.41235	Hsred*	

TamHydS^{ADT} H₂ induced Fig.4

Band position	FWHM	Redox state	Relative amplitude
1895.80284	7.79766	Hred	1
1921.64772	7.45506	Hred	0.26819
2032.02848	11.2203	Hred	0.19558
2063.2198	6.40127	Hred	0.21638
1951.05056	9.58333	HoxH	1
1977.68253	8.56166	HoxH	0.28212
1794.52636	7	HoxH	0.2224
1787.03555	6.74393	Hox	0.18394
1947.18372	5.67991	Hox	1
1970.08406	5.16798	Hox	0.36447
2074.05355	8.77257	Hox	0.18372
2082.33957	7.50004	Hox	0.13168
1802.76391	19.42024	Hred	
1770.15352	14.19617	State 1	0.84244
2071.99269	12.58834	State 1	0.52475
1959.69551	12.02247	State 1	1
1948.61134	10.43683	State 1	0.64005
2090.37639	17.82675	State 1	0.10812
2016.0132	10.72482	State 2	0.46526
1998.96319	11.9203	State 2	1
1852.04096	14.07255	State 2	0.52635
2099.15949	15.93456	State 2	0.35292
2114.43032	5.99389	State 2	0.01017
1759.21076	5.99389	x	
1937.3973	5.99389	x	
1963.84195	5.99389	x	

Supporting References

1. S. T. Stripp, In Situ Infrared Spectroscopy for the Analysis of Gas-processing Metalloenzymes, *Acs Catal*, 2021, **11**, 7845-7862.
2. M. Senger, S. Mebs, J. Duan, F. Wittkamp, U. P. Apfel, J. Heberle, M. Haumann and S. T. Stripp, Stepwise isotope editing of [FeFe]-hydrogenases exposes cofactor dynamics, *Proc Natl Acad Sci U S A*, 2016, **113**, 8454-8459.
3. M. Senger, T. Kernmayr, M. Lorenzi, H. J. Redman and G. Berggren, Hydride state accumulation in native [FeFe]-hydrogenase with the physiological reductant H₂ supports its catalytic relevance, *Chem Commun (Camb)*, 2022, **58**, 7184-7187.
4. M. Senger, S. Mebs, J. Duan, O. Shulenina, K. Laun, L. Kertess, F. Wittkamp, U. P. Apfel, T. Happe, M. Winkler, M. Haumann and S. T. Stripp, Protonation/reduction dynamics at the [4Fe-4S] cluster of the hydrogen-forming cofactor in [FeFe]-hydrogenases, *Phys Chem Chem Phys*, 2018, **20**, 3128-3140.
5. M. Senger, K. Laun, F. Wittkamp, J. Duan, M. Haumann, T. Happe, M. Winkler, U. P. Apfel and S. T. Stripp, Proton-Coupled Reduction of the Catalytic [4Fe-4S] Cluster in [FeFe]-Hydrogenases, *Angew Chem Int Ed Engl*, 2017, **56**, 16503-16506.
6. S. Stoll, in *Multifrequency Electron Paramagnetic Resonance*, 2014, DOI: 10.1002/9783527672431.ch3, pp. 69-138.
7. S. Stoll and A. Schweiger, EasySpin, a comprehensive software package for spectral simulation and analysis in EPR, *J Magn Reson*, 2006, **178**, 42-55.
8. H. Land, A. Sekretareva, P. Huang, H. J. Redman, B. Nemeth, N. Polidori, L. S. Meszaros, M. Senger, S. T. Stripp and G. Berggren, Characterization of a putative sensory [FeFe]-hydrogenase provides new insight into the role of the active site architecture, *Chem Sci*, 2020, **11**, 12789-12801.
9. D. V. Rial and E. A. Ceccarelli, Removal of DnaK contamination during fusion protein purifications, *Protein Expr Purif*, 2002, **25**, 503-507.
10. E. S. Morales, I. L. Parcerisa and E. A. Ceccarelli, A novel method for removing contaminant Hsp70 molecular chaperones from recombinant proteins, *Protein Sci*, 2019, **28**, 800-807.
11. F. Gloaguen, J. D. Lawrence, M. Schmidt, S. R. Wilson and T. B. Rauchfuss, Synthetic and structural studies on [Fe₂(SR)₂(CN)_x(CO)_{6-x}]^(x-) as active site models for Fe-only hydrogenases, *J Am Chem Soc*, 2001, **123**, 12518-12527.
12. C. Esmieu and G. Berggren, Characterization of a monocyanide model of FeFe hydrogenases - highlighting the importance of the bridgehead nitrogen for catalysis, *Dalton Trans*, 2016, **45**, 19242-19248.
13. H. Li and T. B. Rauchfuss, Iron carbonyl sulfides, formaldehyde, and amines condense to give the proposed azadithiolate cofactor of the Fe-only hydrogenases, *J Am Chem Soc*, 2002, **124**, 726-727.
14. H. Land and M. S. Humble, in *Protein Engineering: Methods and Protocols*, eds. U. T. Bornscheuer and M. Höhne, Springer New York, New York, NY, 2018, DOI: 10.1007/978-1-4939-7366-8_4, pp. 43-67.
15. J. Esselborn, N. Muraki, K. Klein, V. Engelbrecht, N. Metzler-Nolte, U. P. Apfel, E. Hofmann, G. Kurisu and T. Happe, A structural view of synthetic cofactor integration into [FeFe]-hydrogenases, *Chem Sci*, 2016, **7**, 959-968.
16. P. R. Cabotaje, K. Walter, A. Zamader, P. Huang, F. Ho, H. Land, M. Senger and G. Berggren, Probing Substrate Transport Effects on Enzymatic Hydrogen Catalysis: An Alternative Proton Transfer Pathway in Putatively Sensory [FeFe] Hydrogenase, *Acs Catal*, 2023, **13**, 10435-10446.
17. N. Chongdar, J. A. Birrell, K. Pawlak, C. Sommer, E. J. Reijerse, O. Rudiger, W. Lubitz and H. Ogata, Unique Spectroscopic Properties of the H-Cluster in a Putative Sensory [FeFe] Hydrogenase, *J Am Chem Soc*, 2018, **140**, 1057-1068.